arXiv:2505.00796v1 [cond-mat.mtrl-sci] 1 May 2025

Beyond kagome: p-bands in kagome metals

Alexander A. Tsirlin[1,*] and Ece Uykur[2,†]

[1] *Felix Bloch Institute for Solid-State Physics, University of Leipzig, 04103 Leipzig, Germany*

[2] *Helmholtz-Zentrum Dresden-Rossendorf, Inst Ion Beam Phys & Mat Res, D-01328 Dresden, Germany*

Abstract

We review recent studies on quantum materials where transition-metal atoms give rise to d-bands typical of kagome metals. Using examples from several material families – AV_3Sb_5, FeGe, RV_6Sn_6, and $LaRu_3Si_2$ – we argue that p-bands contributed by elements beyond the kagome network also play a crucial role in the electronic instabilities, including the charge-density-waves and superconductivity in kagome metals.

* altsirlin@gmail.com

† e.uykur@hzdr.de

I. INTRODUCTION

Materials with layered triangular networks, the so-called kagome metals, became one of the major topics in solid-state research [1–3]. Their interesting properties are traced back to the effect of destructive interference of nearest-neighbor hoppings on the kagome lattice. This effect gives rise to the flat band, the linear Dirac crossing, and the band saddle points that produce van Hove singularities (VHS) in the density of states (Fig. 1). Adjusting the Fermi level to one of these special points creates various instabilities and leads to unusual electronic properties, thus rendering kagome metals prospective quantum materials.

Kagome networks are typically built by transition-metal atoms that give rise to d-bands in the electronic structure. Five d-orbitals per atom result in a plethora of bands that nevertheless still show main features of the nearest-neighbor kagome band structure. Interestingly, these numerous d-bands form only a part of the electronic system of a real material. Hexagonal voids of the kagome network are rarely empty. They are filled by p-elements stabilizing

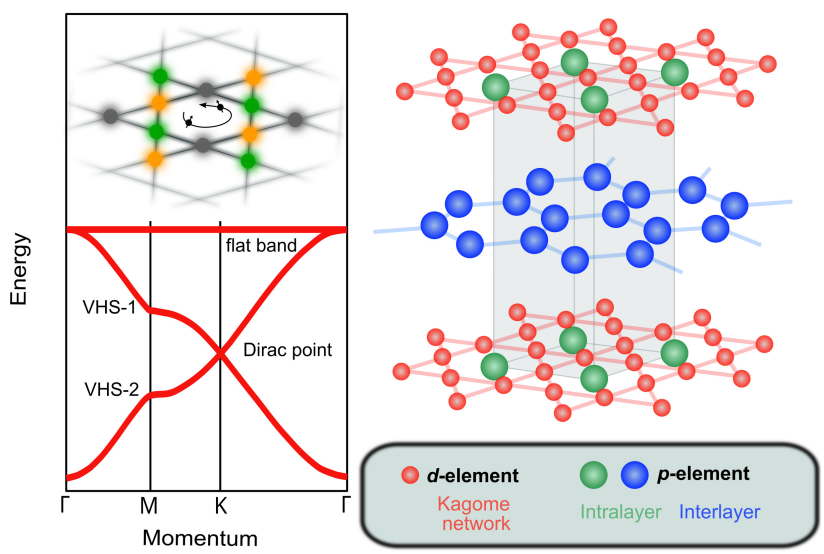

FIG. 1. Left: model band structure of a nearest-neighbor kagome metal features a flat band, a Dirac crossing, and two band saddle points that give rise to van Hove singularities (VHS) in the density of states. Right: real crystal structure that combines the kagome network of a d-metal with p-elements located in the centers of the hexagonal voids ("intralayer") as well as between the kagome layers ("interlayer").

the network. Additionally, p-elements necessarily appear between the kagome layers, usually in the form of hexagonal nets (Fig. 1). The effect of these p-elements on the band structure is different from the behavior known from ionic compounds, such as transition-metal oxides where the p-states of oxygen either lie well below the Fermi level (in Mott insulators) or admix to the d-states via metal-oxygen hybridization (in charge-transfer insulators). Kagome metals show a high degree of covalency, in particular, the direct bonding between the p-elements. This bonding gives rise to the formation of distinct p-bands that will often appear near the Fermi level, produce additional Fermi surfaces, and potentially drive various instabilities concurrent with the native electronic instabilities of the kagome d-bands.

In this Perspective, we review several of the recently studied kagome metals and show that many of their properties should be traced back to the p-states present in the material. We focus on systems with structural phase transitions, which are typically interpreted as charge-density wave (CDW) instabilities of the underlying kagome network. We argue that a complete microscopic understanding of these instabilities requires the treatment of p-states and d-states on equal footing. We also show how the p-bands can be instrumental in tailoring unusual electronic properties of the kagome metals.

II. AV_3SB_5 (A = K, RB, CS)

The AV_3Sb_5 compounds are arguably the most popular family of the kagome metals [4]. They have been extensively covered in a recent review article [5], so we focus on the main aspects only. Two competing instabilities, superconductivity below $T_c = 1 - 3\,\mathrm{K}$ and CDW below T_{CDW} of about $80 - 100\,\mathrm{K}$, are consistently observed in these materials. Electronic structure features prominent V $3d$ bands with several VHS at the M-point of the Brillouin zone within 100 meV from the Fermi level (Fig. 2). The respective microscopic models that include the d-bands with one or several VHS, augmented by the on-site as well as intersite Coulomb repulsion terms, have been the main stage for the theoretical description of AV_3Sb_5. However, an orbital decomposition of the band structure also reveals several bands of the Sb $5p$ origin (Fig. 2). One of these p-bands (Sb1) forms a distinct Fermi surface around Γ. The Sb2 bands hybridize with the V $3d$ bands near M where band saddle points responsible for the VHS are located.

Whereas T_{CDW} of AV_3Sb_5 is rapidly suppressed by pressure and by (most of the) chem-

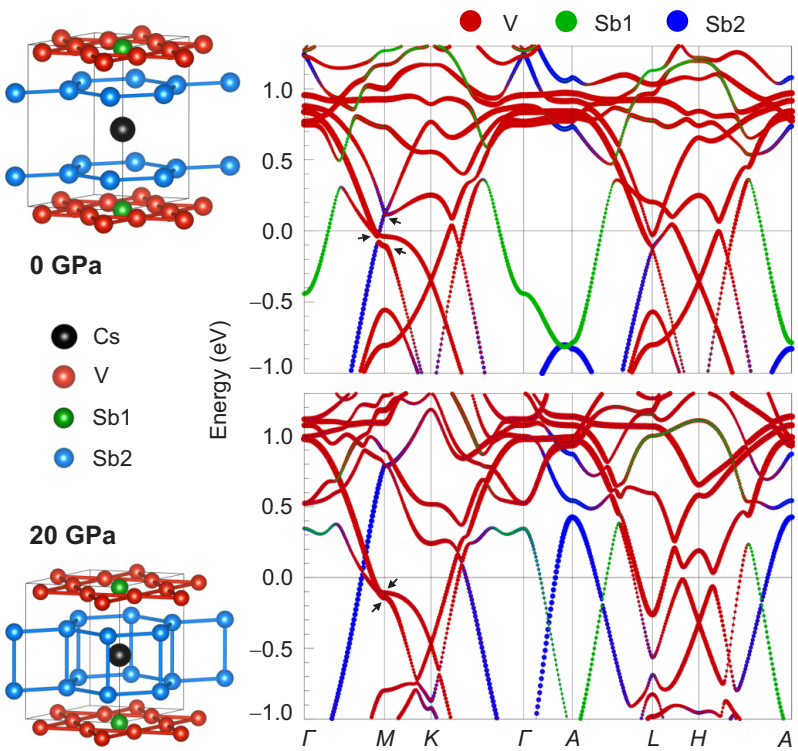

FIG. 2. Pressure-induced 2D–3D crossover in CsV_3Sb_5 [6]: the shrinkage of the c parameter leads to the formation of the interlayer Sb2–Sb2 bonds and a reconstruction of the band structure that mainly affects the Sb1 and Sb2 bands, whereas the kagome d-bands of vanadium show minor changes only. Small arrows denote the band saddle points that give rise to the van Hove singularities near the Fermi level.

ical substitutions, superconductivity remains [5]. It shows a highly unusual behavior, for example as a function of pressure where T_c first increases upon the suppression of the CDW, then decreases once CDW has been eliminated, and then increases again at even higher pressures [7] (Fig. 3a). This reentrant behavior is generic for all three compounds of the AV_3Sb_5 family, with critical pressures increasing upon replacing the smaller A = K atom with the larger Rb or Cs.

Pressure evolution of T_c can be traced back to the changes in the electronic structure. Whereas the d-bands almost do not change under pressure, with the VHS features below the Fermi level being remarkably intact, the p-bands undergo a major reconstruction. The p-band Fermi surface near Γ completely disappears, and a new Fermi surface around A appears at higher pressures [6] (Fig. 2). These changes perfectly correlate with the reentrant behavior of superconductivity, as shown not only by band-structure calculations, but also

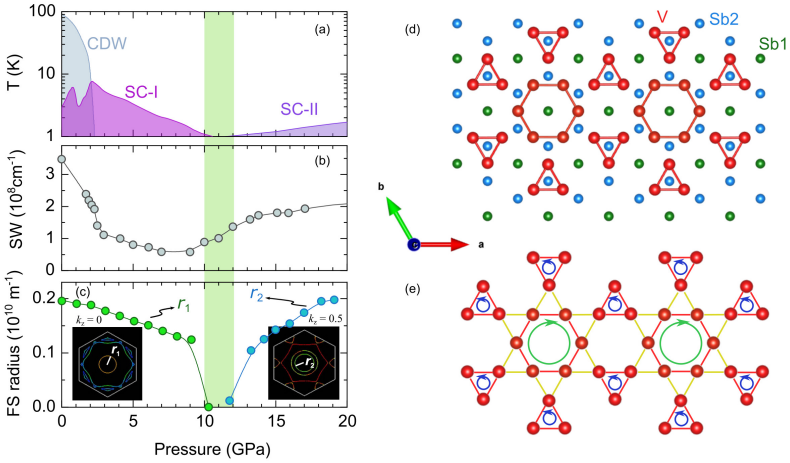

FIG. 3. (a-c) Pressure evolution of CsV_3Sb_5: T_c and T_{CDW} vs. pressure [7] (a), spectral weight of the localization peak as an experimental gauge of electron-phonon coupling [8] (b), and radii of the Sb p-band Fermi surfaces [12] (c). Possible CDW structures: real CDW with the modulation of the V–V bond distances (d), and imaginary CDW with the loop currents (e).

experimentally (Fig. 3b,c). High-pressure infrared spectroscopy demonstrates the nonmonotonic changes in the intraband response that coincide with the pressure evolution of T_c [8]. The origin of this behavior lies in the gradual crossover from the layered 2D structure at ambient pressure to the 3D structure at high pressures. The c parameter shrinks by about 20% between 0 and 20 GPa, thus reducing the distance between the hexagonal Sb nets [6, 9]. The Sb–Sb bonds forming between these nets (Fig. 2) modify the dispersion of the Sb bands and lead to the Fermi surface reconstruction that, in turn, affects the electron-phonon coupling [10] and, eventually, superconductivity [11].

Back to the ambient-pressure regime, superconductivity emerges from the CDW state, which is highly unconventional. Experimentally, the exotic nature of the CDW in AV_3Sb_5 is witnessed by chiral responses and by the anomalous Hall effect that appears below T_{CDW} despite the absence of magnetic order, although time-reversal symmetry breaking may occur [5]. Microscopically, these observations have been understood as a coexistence of a conventional CDW (charge order of the V–V bonds) and an imaginary CDW represented by an orbital magnetic state with loop currents (Fig. 3d,e). Such a complex pair-density wave instability is indeed anticipated in a kagome metal with the filling level near the VHS. Therefore, typical interpretations of the CDW formation in AV_3Sb_5 rely on the nesting be-

tween the VHS proximate to the Fermi level [4]. For example, in CsV_3Sb_5 these VHS are found both slightly below and slightly above the Fermi level at the M-point of the Brillouin zone (Fig. 2).

Several observations challenge this scenario. First, the propagation vectors of the CDW [$\mathbf{q}_1 = (\frac{1}{2}, \frac{1}{2}, \frac{1}{2})$ in KV_3Sb_5 and RbV_3Sb_5, and $\mathbf{q}_2 = (\frac{1}{2}, \frac{1}{2}, \frac{1}{4})$ or a mixture of $\mathbf{q}_1$ and $\mathbf{q}_2$ in CsV_3Sb_5] are not chosen by the Fermi surface nesting [13]. Second, the pressure-induced CDW of CsV_3Sb_5 with the propagation vector $\mathbf{q}_3 = (0, \frac{3}{8}, \frac{1}{2})$ can not be associated with any nesting at all [14]. Third, strain effect on CsV_3Sb_5 leads to a shift of the VHS toward the Fermi level, but the CDW is suppressed [15].

These observations suggest that the VHS alone do not account for the stability of the CDW in AV_3Sb_5. Indeed, Sb atoms provide a major contribution to the stabilization energy of the CDW [16], because any changes in the V–V distances must be accompanied by the displacements of Sb atoms, which are strongly bound to vanadium. Resonant x-ray scattering at the Sb L_1 edge witnesses the involvement of Sb p-states in the CDW formation [17]. Moreover, the suppression of CDW under pressure can be rationalized if one considers that the shrinkage of the c parameter hinders the out-of-plane displacements of Sb, which stabilize the CDW state. By contrast, the VHS and their nesting show no appreciable changes under pressure [6]. Therefore, even if CDW is driven by electronic effects in the d-bands, it is the p-states of Sb that decide on the formation of the CDW, including the choice of its propagation vector and the energy gain compared to the normal state.

One further limitation of the purely d-band scenario becomes clear from the comparison between different members of the AV_3Sb_5 family. While the in-plane lattice parameters of these compounds are almost the same, the c-parameter is strongly influenced by the size of the alkaline metal. The c/a ratio decreases from 1.694 in CsV_3Sb_5 to 1.658 in RbV_3Sb_5 and 1.634 in KV_3Sb_5 at ambient pressure [18]. At first glance, one could consider the Rb and K compounds as the compressed versions of CsV_3Sb_5 corresponding to the nominal pressures of 0.8 and 1.2 GPa, respectively. In this case, the T_{CDW} should be reduced to $40 - 50\,\mathrm{K}$, but in fact it remains at $78\,\mathrm{K}$ in KV_3Sb_5 and even increases to $104\,\mathrm{K}$ in RbV_3Sb_5 compared to $94\,\mathrm{K}$ in CsV_3Sb_5 [5]. The change in the CDW propagation vector is observed as well and may be related to a different sequence of the VHS in the K and Rb vs. Cs compounds, as confirmed spectroscopically [19]. Further work would be needed to elucidate this change also on the microscopic level, but it clearly requires the consideration of the p-states, which

are mainly influenced by the change in c/a, whereas the kagome network itself remains essentially intact.

III. FEGE

In contrast to the AV_3Sb_5 kagome metals discovered only in 2019 [18], hexagonal polymorph of FeGe has been extensively studied already in 1970's and received renewed attention in the recent years in the context of the kagome research. Its main difference from all other materials covered in this Perspective is the presence of the A-type antiferromagnetic order (ferromagnetic layers stacked antiferromagnetically, Fig. 4) below 410 K with a further transition to an incommensurate and canted antiferromagnetic phase below 60 K [20].

A new addition to this already complex behavior is the discovery of yet another transition at 110 K [21] interpreted as a formation of a CDW, based on the observation of the 2×2 in-plane superstructure [21, 22], the partial gap opening below T_{CDW} [23], and the presence of VHS near the Fermi level [23], all reminiscent of AV_3Sb_5. However, an optical probe revealed an enhancement of the low-energy spectral weight in FeGe below T_{CDW} [24], at odds with the typical CDW behavior where spectral weight is transferred from lower to higher energies as a result of the gap opening.

These seemingly conflicting observations could be reconciled using the experimental crystal structure below T_{CDW} where almost no deformation of the Fe kagome layers has been found. The main structural change is due to out-of-plane displacements of the Ge atoms that center the kagome layers [25] (Fig. 4). One quarter of these Ge atoms undergoes dimerization that splits the respective Ge p-band and accounts for the changes in the electronic structure below T_{CDW} [26, 27]. Concurrently, the 2×2 structural modulation folds the Fe d-bands without any significant reconstruction of the Fermi surface [28] and facilitates optical transitions that enhance the low-energy spectral weight [24]. The distortion in the Ge sublattice imposes a structural modulation on the Fe sublattice without gapping out the respective d-bands. This scenario is entirely different from the usual CDW. Indeed, no Kohn anomaly (phonon softening due to electron-phonon coupling) was observed in FeGe. The phonons harden upon cooling through T_{CDW} [29, 30].

The proclivity of the Ge atoms for dimerization appears to be highly sensitive to the distribution of Ge vacancies influenced by post-annealing [31]. This subtlety explains several

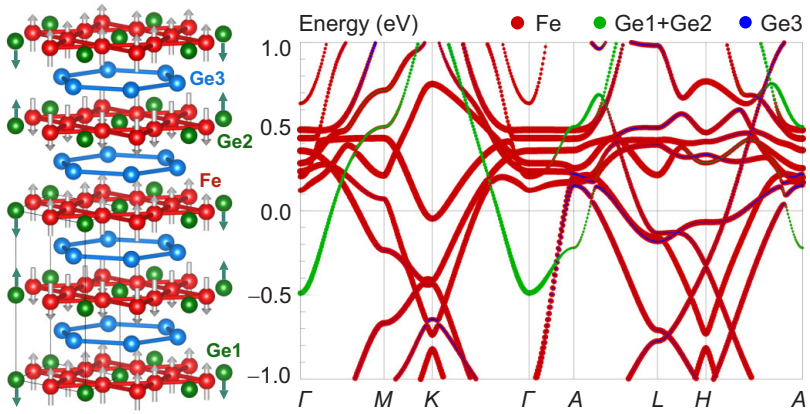

FIG. 4. Left: crystal structure of FeGe with the A-type antiferromagnetic order. The green arrows on the Ge atoms show the displacements below T_{CDW}. Right: band structure of FeGe in the normal state (A-type AFM order) features Fe d-bands along with the p-band formed by the Ge1 and Ge2 atoms.

observations of the dimerized state being either long-range-ordered or only short-range-ordered, with dissimilar manifestations of the transition anomalies at T_{CDW} depending on the thermal treatment of the sample [32, 33].

The transition at T_{CDW} is mainly driven by a spin-phonon coupling [29], the gain in the magnetic energy upon the Ge dimerization [34, 35]. In contrast to the uncorrelated CsV_3Sb_5, FeGe is moderately correlated, as seen from the significant renormalization of the band energies in photoemission [23] and optical [24] spectra compared to density-functional calculations, and further confirmed by a calculation of the on-site Coulomb interactions [36, 37]. Adding correlations is indeed necessary to soften the relevant phonon mode [36, 38], but no such softening happens on approaching T_{CDW} experimentally [29, 30]. The effect of correlations appears to be quantitative and not qualitative, because the low-temperature structure with the dimerized Ge atoms is stable even in the absence of correlations [27, 29, 39]. On the other hand, electronic correlations may be still relevant to some other exotic properties observed in FeGe. Those include the anomalous Hall effect reported below T_{CDW} [21], the prominent edge states detected by scanning tunneling spectroscopy [22], the unusual increase in the crystalline symmetry on cooling across T_{CDW} [40], and the incommensurate spin excitations that appear well above T_{CDW} before condensing into the canted magnetic state below 60 K [41]. The complete microscopic origin of these effects requires further dedicated investigation.

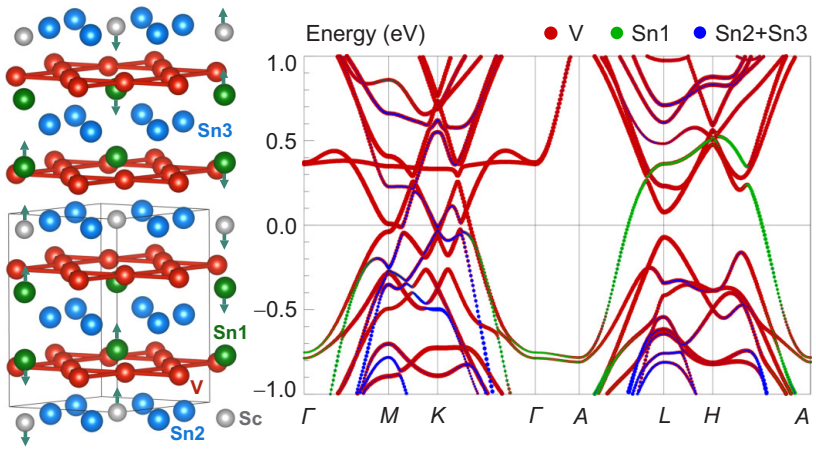

FIG. 5. Left: crystal structure of ScV_6Sn_6 with the arrows showing the atomic displacements in the CDW state [42]. Right: band structure of ScV_6Sn_6 (normal state) near the Fermi level features multiple V $3d$ bands and a separate band with the dominant Sn1 contribution.

IV. RV_6SN_6 (R = SC, Y, LU) AND $LUNB_6SN_6$

Nonmagnetic ScV_6Sn_6 offers an interesting comparison to AV_3Sb_5 because it shows a CDW with the similar T_{CDW} of 92 K, yet no superconductivity [42]. Electronic structure of this compound features multiple VHS of the V d-bands in the vicinity of the Fermi level [43, 44], thus reinforcing the similarity to AV_3Sb_5 and inspiring a similar microscopic interpretation. However, the CDW of ScV_6Sn_6 adopts a different propagation vector of $\mathbf{q} = (\frac{1}{3}, \frac{1}{3}, \frac{1}{3})$ [42] that has not been observed in the AV_3Sb_5 family. The CDW state is mainly characterized by the out-of-plane displacements of the Sc and Sn atoms [42, 45, 46] (Fig. 5).

The bilayer structure of ScV_6Sn_6 gives rise to the Sn p-band crossing the Fermi level (Fig. 5), and mostly these states are affected by the CDW formation [47], whereas the VHS are unchanged below T_{CDW} [48], and no gap opening is seen in the optical spectra [49]. Electron-phonon coupling associated with the Sn p-orbitals was identified as the primary mechanism of this instability [45, 46]. Interestingly, already 5% of the Y or Lu substitution on the Sc site leads to a complete suppression of the CDW [50], whereas pure YV_6Sn_6 and LuV_6Sn_6 do not show any CDW either [51, 52]. These observations were explained by the geometrical effect of the small Sc atoms that allow the out-of-plane displacements of Sn1, whereas larger Y and Lu atoms prevent the displacements of Sn and hinder the

CDW formation. Consistent with these trends, external pressure eliminates the CDW above 2.4 GPa [53], whereas the in-plane compressive strain with the concomitant elongation of the c parameter stabilizes the CDW compared to the strain-free sample [54]. From crystal structure standpoint, the CDW in ScV_6Sn_6 shows intriguing similarities to FeGe where the CDW instability is also caused by the p-element located in the center of the kagome network with almost no impact on the kagome network itself.

In-depth studies of the CDW state of ScV_6Sn_6 revealed further peculiarities, including the anomalous Hall effect [52, 55], possible time-reversal symmetry breaking [56], and various nematic instabilities [57, 58]. The current theoretical interpretation of these phenomena hinges upon the presence of multiple VHS near the Fermi level and the ensuing excitonic order [59]. The underlying assumption is that the Sn p-states become gapped below T_{CDW} and expose the physics of the V d-bands. On the other hand, ScV_6Sn_6 features competing CDW instabilities [45, 60, 61] and strongly anharmonic phonons [62] that are likely to affect the behavior of the material also below T_{CDW}. The role of these effects remains to be explored in future studies.

Recent work on the isostructural Nb-based kagome metals RNb_6Sn_6 (R = rare-earth) uncovered striking similarities to the RV_6Sn_6 family discussed above. Among Nb-based compounds, only $LuNb_6Sn_6$, the compound with the smallest R-cation, shows a CDW instability [63]. It features the same CDW propagation vector as in ScV_6Sn_6 [63], and mostly the Sn p-states are affected by the CDW formation, whereas the Nb d-states are largely intact [64]. External pressure reduces the Lu–Sn distances and suppresses the CDW already above 1.9 GPa [65]. All these observations reinforce the scenario of the Sn atoms and their p-states causing the CDW instability in the 166 kagome metals.

V. LARU$_3$SI$_2$

Similar to AV_3Sb_5, $LaRu_3Si_2$ manifests both CDW and superconductivity. It belongs to a large family of superconducting 132 compounds with the highest T_c of 7 K at ambient pressure. Doping dependence of the T_c [66, 67] along with muon spectroscopy experiments [68] consistently indicate nodeless superconductivity in the parent compound, whereas Fe doping renders superconductivity nodal before completely suppressing it at about 4% substitution [69]. Calculations based on the electron-phonon coupling significantly underestimate

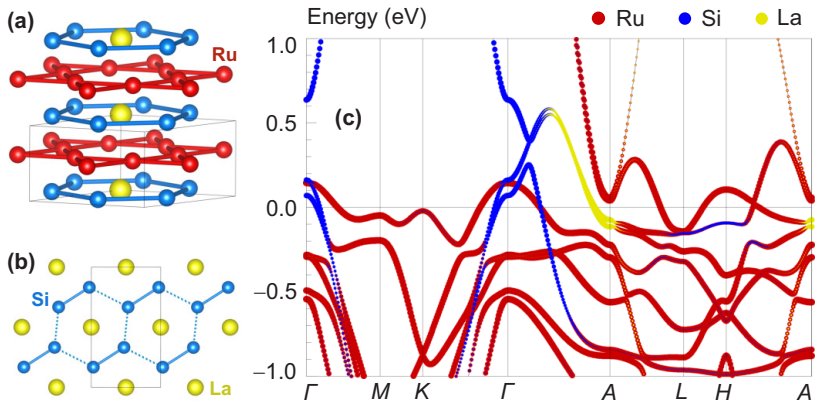

FIG. 6. (a) Hexagonal crystal structure of $LaRu_3Si_2$ above 600 K ($P6/mmm$). (b) Orthorhombic crystal structure below 600 K ($Cccm$) shows the primary deformation mode due to in-plane displacements of Si, resulting in the dimerization of the honeycomb network [71]. (c) Band structure of $LaRu_3Si_2$ calculated using the high-temperature ($P6/mmm$) crystal structure for an easier comparison with other materials.

the T_c [68], indicating a potentially unconventional mechanism of the superconductivity. Indeed, heat capacity of $LaRu_3Si_2$ deviates from the typical metallic behavior suggesting the effect of electronic correlations [69, 70]. Such correlations are usually associated with the presence of weakly dispersive d-bands near the Fermi level. Additionally, VHS typical of a kagome metal appear in the band structure near the M-point (Fig. 6).

The superconductivity in $LaRu_3Si_2$ is intertwined with two concurrent CDW-like instabilities. Below $T_{CO,1} \simeq 400$ K, a structural modulation with $\mathbf{q}_1 = (\frac{1}{4}, 0, 0)$ appears, followed by another structural modulation with $\mathbf{q}_2 = (\frac{1}{6}, 0, 0)$ below $T_{CO,2} \simeq 80$ K, and an additional transition at $T^* \simeq 35$ K of hitherto unknown origin [72]. The increase in the magnetoresistance below $T_{CO,2}$ [72] evokes parallels to the anomalous Hall effect observed in the CDW states of the nominally nonmagnetic AV_3Sb_5 and ScV_6Sn_6. However, in contrast to AV_3Sb_5, the superconducting and putative CDW instabilities in $LaRu_3Si_2$ are clearly synergistic because they show similar evolution under pressure. The superconducting T_c remains around 7 K up to 12 GPa and decreases at higher pressure concomitant with the transformation of the long-range-ordered superstructure into short-range charge correlations [73]. Negative pressure introduced by Ge doping on the Si site increases T_c [74].

Spectroscopic experiments would be required to explore the changes in the electronic structure below $T_{CO,1}$ and $T_{CO,2}$ and the nature of the electronic states that become gapped

in the putative CDW phases. Importantly, though, the normal state of $LaRu_3Si_2$ features strongly intertwined d- and p-bands, similar to the other kagome metals. A dispersive Si $3p$ band is clearly seen in the band structure along with a sizable contribution from La (see Fig. 6), which centers the honeycomb network of Si atoms and participates in the bonding.

Owing to the larger size of Ru, the in-plane lattice parameter of $LaRu_3Si_2$ is increased compared to $3d$ kagome metals. This in-plane stretching results in longer Si–Si distances in the honeycomb network and renders it unstable. Indeed, already at 600 K, above $T_{CO,1}$, $LaRu_3Si_2$ undergoes another structural phase transition with the in-plane dimerization of the Si atoms (Fig. 6) and only a minor impact on the kagome layers [71]. The transition at $T_{CO,1}$ renders the kagome layer more deformed and slightly buckled, but it also involves additional displacements of Si [71], thus making the p-states and associated instabilities a potentially important ingredient of the $LaRu_3Si_2$ physics. Note that $LaRu_3Si_2$ does not feature Si atoms in the kagome layers. Therefore, the primary displacement mode of the p-element is in-plane, in contrast to the out-of-plane modes in ScV_6Sn_6 and FeGe.

VI. CONCLUDING REMARKS

The kagome metals covered in this Perspective are quite different in terms of their energy scales and ground states (Fig. 7), yet they share several commonalities. All these materials feature van Hove singularities that arise from the d-bands and reflect the underlying kagome structure. They also entail distinct p-bands that cross the Fermi level and contribute parts of the Fermi surface. In AV_3Sb_5, the CDW instability gaps out the d-bands near the M-point of the Brillouin zone, while the p-bands remain largely intact. An opposite situation is realized in FeGe and ScV_6Sn_6 where mainly the p-bands become gapped below T_{CDW}, whereas the d-bands do not. Regardless of the exact scenario, the CDW's of kagome metals are quite unusual because a significant part of the Fermi surface is not affected by the CDW transition. The resistivities of AV_3Sb_5 [5], FeGe [33], and ScV_6Sn_6 [42] all decrease below T_{CDW}, likely because of the reduced interband scattering. This behavior is at odds with the conventional expectations for a CDW and may serve as a simple fingerprint of the underlying multi-band scenario with a combination of the d- and p-bands. No structural deformation gaps both of these bands simultaneously.

The variations of T_{CDW} with hydrostatic, uniaxial, and chemical pressure can not be

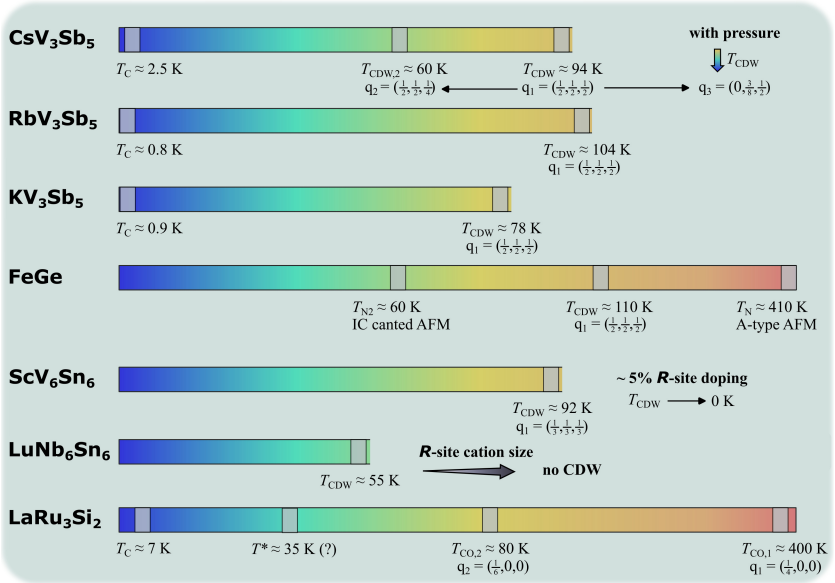

FIG. 7. Summary of the kagome metals reviewed in this Perspective. The critical temperatures of the superconducting and CDW instabilities are indicated, along with the CDW propagation vectors.

accounted for by the changes in the d-band van Hove singularities. Instead, the evolution of CDW in AV_3Sb_5, FeGe, and ScV_6Sn_6 is well explained when the p-elements are taken into account. The out-of-plane displacements of these p-elements are naturally controlled by the interlayer spacing and allow a strong coupling of the CDW to the external stimuli. The d-bands may create electronic pre-conditions for the CDW formation, but the eventual structural distortion and its energy/temperature scale are decided by the p-element. Generically, the 2D kagome network should not be strongly affected by pressure, because in-plane hoppings are rather insensitive to the out-of-plane lattice parameter and c/a ratio. The strong pressure response is rooted in the p-elements that change their position (AV_3Sb_5) or proclivity for dimerization (FeGe, ScV_6Sn_6) with the reduction in c/a. $LaRu_3Si_2$ can be an interesting reference case here, because its leading atomic displacements are in-plane, also for the p-elements. Detailed studies of the CDW's in this compound would be very insightful.

A natural question at this juncture is whether kagome metals without the p-bands are possible at all. In fact, they do exist. Fe_3Sn_2, Ni_3In, RMn_6Sn_6 (R = rare-earth) all lack distinct p-bands in the vicinity of the Fermi level, although they do show some admixture of the p-states to the predominant d-bands. Incidentally, none of these kagome metals exhibits

CDW transitions or any other structural instabilities. This further supports the idea that the p-states must be involved – namely, form distinct bands and parts of the Fermi surface – for a CDW in a kagome metal to occur. An interesting case for future work is the ATi_3Bi_5 family (A = Rb, Cs) where Bi 6p bands make a prominent contribution near the Fermi level [75], no CDW is observed, but signatures of electronic nematicity have been reported [76].

One of the most intriguing features of the kagome metals is their unconventional superconductivity that, at least theoretically, emerges from the various density-wave orders in the kagome d-bands [77]. The ambient-pressure superconductivity of AV_3Sb_5 indeed shows several highly unusual features, such as the abnormal charge-4e and 6e flux quantization [78] and time-reversal symmetry breaking [79]. From the materials perspective, it may be important that many of the carriers reside in the p-band of AV_3Sb_5, whereas the d-bands are at least partially gapped by the CDW. The disappearance of the p-band upon compression or doping is clearly correlated with the suppression of superconductivity [5, 6]. The situation here may be somewhat similar to the CDW: the p-bands are responsible for the stabilization of superconductivity, whereas the d-bands impart more exotic features to it. Including the p-bands within realistic theoretical models would be highly desirable in order to shed further light on this peculiar interplay. The p-states may also be relevant to various subtleties of the AV_3Sb_5 behavior, such as the differences between the strained and strain-free samples [80] or between the bulk samples and thin flakes [81], because external stimuli are more likely to couple to the p-states than to the kagome network itself.

From the materials design perspective, the p-elements of kagome metals offer an excellent opportunity of controlling the CDW. Chemical substitutions in the p-sublattice and even in the A-sublattice, as in the case of ScV_6Sn_6, can be used to suppress CDW with only a minor impact on the kagome d-bands. An ultimate example of this control is FeGe where the appearance of the structural instability and its long-range vs. short-range nature hinge upon the distribution of Ge vacancies in the sample. A periodic drive affecting the p-elements, for example via exciting a phonon mode related to these atoms, may be another interesting way of controlling the CDW in kagome metals.

In summary, the p-elements and their corresponding p-bands are an integral part of kagome metals. They enrich the physics of these quantum materials and offer ample opportunities for controlling the electronic states therein.

TECHNICAL NOTES

All band structures shown in this work are calculated with the `FPLO` code [82] on the full-relativistic level using the Perdew-Burke-Ernzerhof exchange-correlation potential [83] and experimental structural parameters. `VESTA` program was used for crystal structure visualization [84].

ACKNOWLEDGMENTS

We thank Maxim Wenzel and Martin Dressel for the long-term collaboration on the optical studies of kagome metals, as well as Brenden Ortiz, Stephen Wilson, Claudia Felser, David Mandrus, and Hechang Lei for providing the crystals of these interesting materials. We are also grateful to the Deutsche Forschungsgemeinschaft (DFG, German Research Foundation) for the funding under TRR 360 (492547816) and UY63/2-1.

---

[1] J.-X. Yin, B. Lian, and M. Z. Hasan, Topological kagome magnets and superconductors, Nature **612**, 647 (2022).

[2] Y. Wang, H. Wu, G. T. McCandless, J. Y. Chan, and M. N. Ali, Quantum states and intertwining phases in kagome materials, Nature Rev. Physics **5**, 635 (2023).

[3] Q. Wang, H. Lei, Y. Qi, and C. Felser, Topological quantum materials with kagome lattice, Acc. Mater. Res. **5**, 786 (2024).

[4] T. Neupert, M. M. Denner, J.-X. Yin, R. Thomale, and M. Z. Hasan, Charge order and superconductivity in kagome materials, Nature Phys. **18**, 137 (2022).

[5] S. D. Wilson and B. R. Ortiz, AV_3Sb_5 kagome superconductors, Nature Rev. Materials **9**, 420 (2024).

[6] A. A. Tsirlin, P. Fertey, B. R. Ortiz, B. Klis, V. Merkl, M. Dressel, S. D. Wilson, and E. Uykur, Role of Sb in the superconducting kagome metal CsV_3Sb_5 revealed by its anisotropic compression, SciPost Phys. **12**, 049 (2022).

[7] Y. Zhou, G. Ye, S. Luo, Y. Song, X. Lu, and H. Yuan, Kagome materials AV_3Sb_5 (A = K, Rb, Cs): pairing symmetry and pressure-tuning studies, Supercond. Sci. Tech. **37**, 103001 (2024).

[8] M. Wenzel, A. A. Tsirlin, F. Capitani, Y. T. Chan, B. R. Ortiz, S. D. Wilson, M. Dressel, and E. Uykur, Pressure evolution of electron dynamics in the superconducting kagome metal CsV_3Sb_5, npj Quant. Mater. **8**, 45 (2023).

[9] F. Yu, X. Zhu, X. Wen, Z. Gui, Z. Li, Y. Han, T. Wu, Z. Wang, Z. Xiang, Z. Qiao, J. Ying, and X. Chen, Pressure-induced dimensional crossover in a kagome superconductor, Phys. Rev. Lett. **128**, 077001 (2022).

[10] J.-G. Si, W.-J. Lu, Y.-P. Sun, P.-F. Liu, and B.-T. Wang, Charge density wave and pressure-dependent superconductivity in the kagome metal CsV_3Sb_5: A first-principles study, Phys. Rev. B **105**, 024517 (2022).

[11] E. T. Ritz, H. S. Røising, M. H. Christensen, T. Birol, B. M. Andersen, and R. M. Fernandes, Superconductivity from orbital-selective electron-phonon coupling in AV_3Sb_5, Phys. Rev. B **108**, L100510 (2023).

[12] A. A. Tsirlin, B. R. Ortiz, M. Dressel, S. D. Wilson, S. Winnerl, and E. Uykur, Effect of nonhydrostatic pressure on the superconducting kagome metal CsV_3Sb_5, Phys. Rev. B **107**, 174107 (2023).

[13] F. Kaboudvand, S. M. L. Teicher, S. D. Wilson, R. Seshadri, and M. D. Johannes, Fermi surface nesting and the lindhard response function in the kagome superconductor csv_3sb_5, Appl. Phys. Lett. **120**, 111901 (2022).

[14] F. Stier, A.-A. Haghighirad, G. Garbarino, S. Mishra, N. Stilkerich, D. Chen, C. Shekhar, T. Lacmann, C. Felser, T. Ritschel, J. Geck, and M. Le Tacon, Pressure-dependent electronic superlattice in the kagome superconductor CsV_3Sb_5, Phys. Rev. Lett. **133**, 236503 (2024).

[15] C. Lin, A. Consiglio, O. K. Forslund, J. Küspert, M. M. Denner, H. Lei, A. Louat, M. D. Watson, T. K. Kim, C. Cacho, D. Carbone, M. Leandersson, C. Polley, T. Balasubramanian, D. D. Sante, R. Thomale, Z. Guguchia, G. Sangiovanni, T. Neupert, and J. Chang, Uniaxial strain tuning of charge modulation and singularity in a kagome superconductor, Nature Comm. **15**, 10466 (2024).

[16] E. T. Ritz, R. M. Fernandes, and T. Birol, Impact of Sb degrees of freedom on the charge density wave phase diagram of the kagome metal CsV_3Sb_5, Phys. Rev. B **107**, 205131 (2023).

[17] H. Li, G. Fabbris, A. H. Said, J. P. Sun, Y.-X. Jiang, J.-X. Yin, Y.-Y. Pai, S. Yoon, A. R. Lupini, C. S. Nelson, Q. W. Yin, C. S. Gong, Z. J. Tu, H. C. Lei, J.-G. Cheng, M. Z. Hasan, Z. Wang, B. Yan, R. Thomale, H. N. Lee, and H. Miao, Discovery of conjoined charge density

waves in the kagome superconductor CsV_3Sb_5, Nature Comm. **13**, 6348 (2022).

[18] B. R. Ortiz, L. C. Gomes, J. R. Morey, M. Winiarski, M. Bordelon, J. S. Mangum, I. W. H. Oswald, J. A. Rodriguez-Rivera, J. R. Neilson, S. D. Wilson, E. Ertekin, T. M. McQueen, and E. S. Toberer, New kagome prototype materials: discovery of KV_3Sb_5, RbV_3Sb_5, and CsV_3Sb_5, Phys. Rev. Materials **3**, 094407 (2019).

[19] M. Wenzel, B. R. Ortiz, S. D. Wilson, M. Dressel, A. A. Tsirlin, and E. Uykur, Optical study of RbV_3Sb_5: Multiple density-wave gaps and phonon anomalies, Phys. Rev. B **105**, 245123 (2022).

[20] J. Bernhard, B. Lebech, and O. Beckman, Neutron diffraction studies of the low-temperature magnetic structure of hexagonal FeGe, J. Phys. F **14**, 2379 (1984).

[21] X. Teng, L. Chen, F. Ye, E. Rosenberg, Z. Liu, J.-X. Yin, Y.-X. Jiang, J. S. Oh, M. Z. Hasan, K. J. Neubauer, B. Gao, Y. Xie, M. Hashimoto, D. Lu, C. Jozwiak, A. Bostwick, E. Rotenberg, R. J. Birgeneau, J.-H. Chu, M. Yi, and P. Dai, Discovery of charge density wave in a kagome lattice antiferromagnet, Nature **609**, 490 (2022).

[22] J.-X. Yin, Y.-X. Jiang, X. Teng, M. S. Hossain, S. Mardanya, T.-R. Chang, Z. Ye, G. Xu, M. M. Denner, T. Neupert, B. Lienhard, H.-B. Deng, C. Setty, Q. Si, G. Chang, Z. Guguchia, B. Gao, N. Shumiya, Q. Zhang, T. A. Cochran, D. Multer, M. Yi, P. Dai, and M. Z. Hasan, Discovery of charge order and corresponding edge state in kagome magnet FeGe, Phys. Rev. Lett. **129**, 166401 (2022).

[23] X. Teng, J. S. Oh, H. Tan, L. Chen, J. Huang, B. Gao, J.-X. Yin, J.-H. Chu, M. Hashimoto, D. Lu, C. Jozwiak, A. Bostwick, E. Rotenberg, G. E. Granroth, B. Yan, R. J. Birgeneau, P. Dai, and M. Yi, Magnetism and charge density wave order in kagome FeGe, Nature Phys. **19**, 814 (2023).

[24] M. Wenzel, E. Uykur, A. A. Tsirlin, S. Pal, R. M. Roy, C. Yi, C. Shekhar, C. Felser, A. V. Pronin, and M. Dressel, Intriguing low-temperature phase in the antiferromagnetic kagome metal FeGe, Phys. Rev. Lett. **132**, 266505 (2024).

[25] Z. Chen, X. Wu, S. Zhou, J. Zhang, R. Yin, Y. Li, M. Li, J. Gong, M. He, Y. Chai, X. Zhou, Y. Wang, A. Wang, Y.-J. Yan, and D.-L. Feng, Discovery of a long-ranged charge order with 1/4 Ge1-dimerization in an antiferromagnetic kagome metal, Nature Comm. **15**, 6262 (2024).

[26] Z. Zhao, T. Li, P. Li, X. Wu, J. Yao, Z. Chen, Y. Yan, S. Cui, Z. Sun, Y. Yang, Z. Jiang, Z. Liu, A. Louat, T. Kim, C. Cacho, A. Wang, Y. Wang, D. Shen, J. Jiang, and D. Feng,

Photoemission evidence of a novel charge order in kagome metal FeGe, Sci. China Phys. Mech. Astr. **68**, 267012 (2025).

[27] H. Tan and B. Yan, Disordered charge density waves in the kagome metal FeGe, Phys. Rev. B **111**, 045160 (2025).

[28] K. Tang, H. Zhou, H. Li, S. Pan, X. Wu, H. Li, N. Zhang, C. Xi, J. Zhang, A. Wang, X. Wan, Z. Xiang, and X. Chen, Evidence for unfolded fermi surfaces in the charge-density-wave state of kagome metal FeGe revealed by de Haas-van Alphen effect, Phys. Rev. Research **6**, 013276 (2024).

[29] H. Miao, T. T. Zhang, H. X. Li, G. Fabbris, A. H. Said, R. Tartaglia, T. Yilmaz, E. Vescovo, J.-X. Yin, S. Murakami, X. L. Feng, K. Jiang, X. L. Wu, A. F. Wang, S. Okamoto, Y. L. Wang, and H. N. Lee, Signature of spin-phonon coupling driven charge density wave in a kagome magnet, Nature Comm. **14**, 6183 (2023).

[30] X. Teng, D. W. Tam, L. Chen, H. Tan, Y. Xie, B. Gao, G. E. Granroth, A. Ivanov, P. Bourges, B. Yan, M. Yi, and P. Dai, Spin-charge-lattice coupling across the charge density wave transition in a kagome lattice antiferromagnet, Phys. Rev. Lett. **133**, 046502 (2024).

[31] M. L. Klemm, S. Siddique, Y.-C. Chang, S. Xu, Y. Xie, T. Legvold, M. T. Kiani, X. Teng, B. Gao, F. Ye, H. Cao, Y. Hao, W. Tian, H. Luetkens, M. Matsuda, D. Natelson, Z. Guguchia, C.-L. Huang, M. Yi, J. J. Cha, and P. Dai, Vacancy-induced suppression of charge density wave order and its impact on magnetic order in kagome antiferromagnet FeGe, Nature Comm. **16**, 3313 (2025).

[32] X. Wu, X. Mi, L. Zhang, C.-W. Wang, N. Maraytta, X. Zhou, M. He, M. Merz, Y. Chai, and A. Wang, Annealing-tunable charge density wave in the magnetic kagome material FeGe, Phys. Rev. Lett. **132**, 256501 (2024).

[33] C. Shi, Y. Liu, B. B. Maity, Q. Wang, S. R. Kotla, S. Ramakrishnan, C. Eisele, H. Agarwal, L. Noohinejad, Q. Tao, B. Kang, Z. Lou, X. Yang, Y. Qi, X. Lin, Z.-A. Xu, A. Thamizhavel, G.-H. Cao, S. van Smaalen, S. Cao, and J.-K. Bao, Annealing-induced long-range charge density wave order in magnetic kagome FeGe: Fluctuations and disordered structure, Sci. China Phys. Mech. Astr. **67**, 117012 (2024).

[34] Y. Wang, Enhanced spin-polarization via partial Ge-dimerization as the driving force of the charge density wave in FeGe, Phys. Rev. Materials **7**, 104006 (2023).

[35] S. Shao, J.-X. Yin, I. Belopolski, J.-Y. You, T. Hou, H. Chen, Y. Jiang, M. S. Hossain, M. Yahyavi, C.-H. Hsu, Y. P. Feng, A. Bansil, M. Z. Hasan, and G. Chang, Intertwining of magnetism and charge ordering in kagome FeGe, ACS Nano **17**, 10164 (2023).

[36] H.-Y. Ma, J.-X. Yin, M. Z. Hasan, and J. Liu, Theory for charge density wave and orbital-flux state in antiferromagnetic kagome metal FeGe, Chin. Phys. Lett. **41**, 047103 (2024).

[37] Y. Jiang, H. Hu, D. Călugăru, C. Felser, S. Blanco-Canosa, H. Weng, Y. Xu, and B. A. Bernevig, FeGe as a building block for the kagome 1:1, 1:6:6, and 1:3:5 families: Hidden d-orbital decoupling of flat band sectors, effective models, and interaction Hamiltonians, Phys. Rev. B **111**, 125163 (2025).

[38] A. Ptok, S. Basak, A. Kobiałka, M. Sternik, J. Łażewski, P. T. Jochym, A. M. Oleś, and P. Piekarz, Lattice dynamics study of electron-correlation-induced charge density wave in antiferromagnetic kagome metal FeGe, Phys. Rev. Materials **8**, L080601 (2024).

[39] B. Zhang, J. Ji, C. Xu, and H. Xiang, Electronic and magnetic origins of unconventional charge density wave in kagome FeGe, Phys. Rev. B **110**, 125139 (2024).

[40] S. Wu, M. L. Klemm, J. Shah, E. T. Ritz, C. Duan, X. Teng, B. Gao, F. Ye, M. Matsuda, F. Li, X. Xu, M. Yi, T. Birol, P. Dai, and G. Blumberg, Symmetry breaking and ascending in the magnetic kagome metal FeGe, Phys. Rev. X **14**, 011043 (2024).

[41] L. Chen, X. Teng, H. Tan, B. L. Winn, G. E. Granroth, F. Ye, D. H. Yu, R. A. Mole, B. Gao, B. Yan, M. Yi, and P. Dai, Competing itinerant and local spin interactions in kagome metal FeGe, Nature Comm. **15**, 1918 (2024).

[42] H. W. S. Arachchige, W. R. Meier, M. Marshall, T. Matsuoka, R. Xue, M. A. McGuire, R. P. Hermann, H. Cao, and D. Mandrus, Charge density wave in kagome lattice intermetallic ScV_6Sn_6, Phys. Rev. Lett. **129**, 216402 (2022).

[43] Y. Hu, J. Ma, Y. Li, Y. Jiang, D. J. Gawryluk, T. Hu, J. Teyssier, V. Multian, Z. Yin, S. Xu, S. Shin, I. Plokhikh, X. Han, N. C. Plumb, Y. Liu, J.-X. Yin, Z. Guguchia, Y. Zhao, A. P. Schnyder, X. Wu, E. Pomjakushina, M. Z. Hasan, N. Wang, and M. Shi, Phonon promoted charge density wave in topological kagome metal ScV_6Sn_6, Nature Comm. **15**, 1658 (2024).

[44] Z.-J. Cheng, S. Shao, B. Kim, T. A. Cochran, X. P. Yang, C. Yi, Y.-X. Jiang, J. Zhang, M. S. Hossain, S. Roychowdhury, T. Yilmaz, E. Vescovo, A. Fedorov, C. Shekhar, C. Felser, G. Chang, and M. Z. Hasan, Untangling charge-order dependent bulk states from surface effects in a topological kagome metal ScV_6Sn_6, Phys. Rev. B **109**, 075150 (2024).

[45] A. Korshunov, H. Hu, D. Subires, Y. Jiang, D. Călugăru, X. Feng, A. Rajapitamahuni, C. Yi, S. Roychowdhury, M. G. Vergniory, J. Strempfer, C. Shekhar, E. Vescovo, D. Chernyshov, A. H. Said, A. Bosak, C. Felser, B. A. Bernevig, and S. Blanco-Canosa, Softening of a flat phonon mode in the kagome ScV_6Sn_6, Nature Comm. **14**, 6646 (2023).

[46] H. Hu, Y. Jiang, D. Călugăru, X. Feng, D. Subires, M. G. Vergniory, C. Felser, S. Blanco-Canosa, and B. A. Bernevig, Flat phonon soft modes and unconventional charge density wave formation in ScV_6Sn_6: Microscopic and effective theory, Phys. Rev. B **111**, 054113 (2025).

[47] S. Lee, C. Won, J. Kim, J. Yoo, S. Park, J. Denlinger, C. Jozwiak, A. Bostwick, E. Rotenberg, R. Comin, M. Kang, and J.-H. Park, Nature of charge density wave in kagome metal ScV_6Sn_6, npj Quant. Materials **9**, 15 (2024).

[48] D. W. Kim, S. Liu, C. Wang, H. W. Nam, G. Pokharel, S. D. Wilson, J.-H. Cho, and S. J. Moon, Infrared probe of the charge density wave gap in ScV_6Sn_6, Phys. Rev. B **108**, 205118 (2023).

[49] T. Hu, H. Pi, S. Xu, L. Yue, Q. Wu, Q. Liu, S. Zhang, R. Li, X. Zhou, J. Yuan, D. Wu, T. Dong, H. Weng, and N. Wang, Optical spectroscopy and band structure calculations of the structural phase transition in the vanadium-based kagome metal ScV_6Sn_6, Phys. Rev. B **107**, 165119 (2023).

[50] W. R. Meier, R. P. Madhogaria, S. Mozaffari, M. Marshall, D. E. Graf, M. A. McGuire, H. W. S. Arachchige, C. L. Allen, J. Driver, H. Cao, and D. Mandrus, Tiny Sc allows the chains to rattle: Impact of Lu and Y doping on the charge-density wave in ScV_6Sn_6, J. Amer. Chem. Soc. **145**, 20943 (2023).

[51] G. Pokharel, S. M. L. Teicher, B. R. Ortiz, P. M. Sarte, G. Wu, S. Peng, J. He, R. Seshadri, and S. D. Wilson, Electronic properties of the topological kagome metals YV_6Sn_6 and GdV_6Sn_6, Phys. Rev. B **104**, 235139 (2021).

[52] S. Mozaffari, W. R. Meier, R. P. Madhogaria, N. Peshcherenko, S.-H. Kang, J. W. Villanova, H. W. S. Arachchige, G. Zheng, Y. Zhu, K.-W. Chen, K. Jenkins, D. Zhang, A. Chan, L. Li, M. Yoon, Y. Zhang, and D. G. Mandrus, Universal sublinear resistivity in vanadium kagome materials hosting charge density waves, Phys. Rev. B **110**, 035135 (2024).

[53] X. Zhang, J. Hou, W. Xia, Z. Xu, P. Yang, A. Wang, Z. Liu, J. Shen, H. Zhang, X. Dong, Y. Uwatoko, J. Sun, B. Wang, Y. Guo, and J. Cheng, Destabilization of the charge density wave and the absence of superconductivity in ScV_6Sn_6 under high pressures up to 11 GPa,

Materials **15**, 7372 (2022).

[54] M. Tuniz, A. Consiglio, G. Pokharel, F. Parmigiani, T. Neupert, R. Thomale, S. K. Chaluvadi, P. Orgiani, G. Sangiovanni, S. D. Wilson, I. Vobornik, F. Salvador, F. Cilento, D. Di Sante, and F. Mazzola, Strain-induced enhancement of the charge density wave in the kagome metal ScV_6Sn_6, Phys. Rev. Lett. **134**, 066501 (2025).

[55] C. Yi, X. Feng, N. Mao, P. Yanda, S. Roychowdhury, Y. Zhang, C. Felser, and C. Shekhar, Quantum oscillations revealing topological band in kagome metal ScV_6Sn_6, Phys. Rev. B **109**, 035124 (2024).

[56] Z. Guguchia, D. J. Gawryluk, S. Shin, Z. Hao, C. Mielke III, D. Das, I. Plokhikh, L. Liborio, J. K. Shenton, Y. Hu, V. Sazgari, M. Medarde, H. Deng, Y. Cai, C. Chen, Y. Jiang, A. Amato, M. Shi, M. Z. Hasan, J.-X. Yin, R. Khasanov, E. Pomjakushina, and H. Luetkens, Hidden magnetism uncovered in a charge ordered bilayer kagome material ScV_6Sn_6, Nature Comm. **14**, 7796 (2023).

[57] Y.-X. Jiang, S. Shao, W. Xia, M. M. Denner, J. Ingham, M. S. Hossain, Q. Qiu, X. Zheng, H. Chen, Z.-J. Cheng, X. P. Yang, B. Kim, J.-X. Yin, S. Zhang, M. Litskevich, Q. Zhang, T. A. Cochran, Y. Peng, G. Chang, Y. Guo, R. Thomale, T. Neupert, and M. Z. Hasan, Van Hove annihilation and nematic instability on a kagome lattice, Nature Mater. **23**, 1214 (2024).

[58] C. Farhang, W. R. Meier, W. Lu, J. Li, Y. Wu, S. Mozaffari, R. P. Madhogaria, Y. Zhang, D. Mandrus, and J. Xia, Discovery of an intermediate nematic state in a bilayer kagome metal ScV_6Sn_6, arXiv:2502.14568.

[59] J. Ingham, A. Consiglio, D. di Sante, R. Thomale, and H. D. Scammell, Theory of excitonic order in kagome metals ScV_6Sn_6 and $LuNb_6Sn_6$, arXiv:2410.16365.

[60] H. Tan and B. Yan, Abundant lattice instability in kagome metal ScV_6Sn_6, Phys. Rev. Lett. **130**, 266402 (2023).

[61] S. Cao, C. Xu, H. Fukui, T. Manjo, Y. Dong, M. Shi, Y. Liu, C. Cao, and Y. Song, Competing charge-density wave instabilities in the kagome metal ScV_6Sn_6, Nature Comm. **14**, 7671 (2023).

[62] K. Wang, S. Chen, S.-W. Kim, and B. Monserrat, Origin of competing charge density waves in kagome metal ScV_6Sn_6, Nature Comm. **15**, 10428 (2024).

[63] B. R. Ortiz, W. R. Meier, G. Pokharel, J. Chamorro, F. Yang, S. Mozaffari, A. Thaler, S. J. G. Alvarado, H. Zhang, D. S. Parker, G. D. Samolyuk, J. A. M. Paddison, J. Yan, F. Ye,

S. Sarker, S. D. Wilson, H. Miao, D. Mandrus, and M. A. McGuire, Stability frontiers in the AM_6X_6 kagome metals: The $LnNb_6Sn_6$ (Ln:Ce–Lu,Y) family and density-wave transition in $LuNb_6Sn_6$, J. Amer. Chem. Soc. **147**, 5279 (2025).

[64] R. Lou, Y. Zhang, E. Cheng, X. Feng, A. Fedorov, Z. Li, Y. Luo, A. Generalov, H. Ma, Q. Wei, Y. Zhou, S. Changdar, W. Schnelle, D. Chen, Y. Chen, J. Liu, Y. Guo, S. Borisenko, D. V. Vyalikh, C. Felser, B. Büchner, and Z. Liu, Orbital-selective band modifications in a charge-ordered kagome metal $LuNb_6Sn_6$, arXiv:2504.04019.

[65] W. R. Meier, D. E. Graf, B. R. Ortiz, S. Mozaffari, and D. Mandrus, Pressure suppresses the density wave order in kagome metal $LuNb_6Sn_6$, arXiv:2502.04197.

[66] B. Li, S. Li, and H.-H. Wen, Chemical doping effect in the $LaRu_3Si_2$ superconductor with a kagome lattice, Phys. Rev. B **94**, 094523 (2016).

[67] S. Chakrabortty, R. Kumar, and N. Mohapatra, Effect of tunable spin-orbit coupling on the superconducting properties of $LaRu_3Si_2$ containing kagome-honeycomb layers, Phys. Rev. B **107**, 024503 (2023).

[68] C. Mielke, Y. Qin, J.-X. Yin, H. Nakamura, D. Das, K. Guo, R. Khasanov, J. Chang, Z. Q. Wang, S. Jia, S. Nakatsuji, A. Amato, H. Luetkens, G. Xu, M. Z. Hasan, and Z. Guguchia, Nodeless kagome superconductivity in $LaRu_3Si_2$, Phys. Rev. Materials **5**, 034803 (2021).

[69] C. Mielke, D. Das, J. Spring, H. Nakamura, S. Shin, H. Liu, V. Sazgari, S. Jöhr, J. Lyu, J. N. Graham, T. Shiroka, M. Medarde, M. Z. Hasan, S. Nakatsuji, R. Khasanov, D. J. Gawryluk, H. Luetkens, and Z. Guguchia, Microscopic study of the impurity effect in the kagome superconductor $La(Ru_{1-x}Fe_x)_3Si_2$, Phys. Rev. B **109**, 134501 (2024).

[70] S. Li, B. Zeng, X. Wan, J. Tao, F. Han, H. Yang, Z. Wang, and H.-H. Wen, Anomalous properties in the normal and superconducting states of $LaRu_3Si_2$, Phys. Rev. B **84**, 214527 (2011).

[71] I. Plokhikh, C. Mielke III, H. Nakamura, V. Petricek, Y. Qin, V. Sazgari, J. Küspert, I. Biało, S. Shin, O. Ivashko, J. N. Graham, M. v. Zimmermann, M. Medarde, A. Amato, R. Khasanov, H. Luetkens, M. H. Fischer, M. Z. Hasan, J.-X. Yin, T. Neupert, J. Chang, G. Xu, S. Nakatsuji, E. Pomjakushina, D. J. Gawryluk, and Z. Guguchia, Discovery of charge order above room-temperature in the prototypical kagome superconductor $La(Ru_{1-x}Fe_x)_3Si_2$, Comm. Phys. **7**, 182 (2024).

[72] C. Mielke III, V. Sazgari, I. Plokhikh, S. Shin, H. Nakamura, J. N. Graham, J. Küspert, I. Bialo, G. Garbarino, D. Das, M. Medarde, M. Bartkowiak, S. S. Islam, R. Khasanov, H. Luetkens, M. Z. Hasan, E. Pomjakushina, J.-X. Yin, M. H. Fischer, J. Chang, T. Neupert, S. Nakatsuji, B. Wehinger, D. J. Gawryluk, and Z. Guguchia, Charge orders with distinct magnetic response in a prototypical kagome superconductor $LaRu_3Si_2$, arXiv:2402.16219.

[73] K. Ma, I. Plokhikh, J. N. Graham, C. Mielke III, V. Sazgari, H. Nakamura, S. S. Islam, S. Shin, P. Kral, O. Gerguri, H. Luetkens, F. O. von Rohr, J.-X. Yin, E. Pomjakushina, C. Felser, S. Nakatsuji, B. Wehinger, D. J. Gawryluk, S. Medvedev, and Z. Guguchia, Dome-shaped superconducting phase diagram linked to charge order in $LaRu_3Si_2$, arXiv:2412.05459.

[74] R. Misawa, M. Kriener, R. Yamada, R. Nakano, M. Jovanovic, L. M. Schoop, and M. Hirschberger, Chemical enhancement of superconductivity in $LaRu_3Si_2$ with mode-selective coupling between kagome phonons and flat bands, arXiv:2503.22477.

[75] M. Wenzel, E. Uykur, A. A. Tsirlin, A. N. Capa Salinas, B. R. Ortiz, S. D. Wilson, and M. Dressel, Interplay of *d*- and *p*-states in $RbTi_3Bi_5$ and $CsTi_3Bi_5$ flat-band kagome metals, arXiv:2501.18389.

[76] Y. Hu, C. Le, X. Wu, and M. Shi, Topological electronic structure and electronic nematicity in candidate kagome superconductors, ATi_3Bi_5 (A = Rb, Cs), Supercond. Sci. Tech. **37**, 123004 (2024).

[77] M. L. Kiesel, C. Platt, and R. Thomale, Unconventional fermi surface instabilities in the kagome Hubbard model, Phys. Rev. Lett. **110**, 126405 (2013).

[78] J. Ge, P. Wang, Y. Xing, Q. Yin, A. Wang, J. Shen, H. Lei, Z. Wang, and J. Wang, Charge-4e and charge-6e flux quantization and higher charge superconductivity in kagome superconductor ring devices, Phys. Rev. X **14**, 021025 (2024).

[79] H. Deng, G. Liu, Z. Guguchia, T. Yang, J. Liu, Z. Wang, Y. Xie, S. Shao, H. Ma, W. Liége, F. Bourdarot, X.-Y. Yan, H. Qin, C. Mielke III, R. Khasanov, H. Luetkens, X. Wu, G. Chang, J. Liu, M. H. Christensen, A. Kreisel, B. M. Andersen, W. Huang, Y. Zhao, P. Bourges, Y. Yao, P. Dai, and J.-X. Yin, Evidence for time-reversal symmetry-breaking kagome superconductivity, Nature Mater. **23**, 1639 (2024).

[80] C. Guo, G. Wagner, C. Putzke, D. Chen, K. Wang, L. Zhang, M. Gutierrez-Amigo, I. Errea, M. G. Vergniory, C. Felser, M. H. Fischer, T. Neupert, and P. J. W. Moll, Correlated order at the tipping point in the kagome metal CsV_3Sb_5, Nature Phys. **20**, 579 (2024).

[81] B. Song, T. Ying, X. Wu, W. Xia, Q. Yin, Q. Zhang, Y. Song, X. Yang, J. Guo, L. Gu, X. Chen, J. Hu, A. P. Schnyder, H. Lei, Y. Guo, and S. Li, Anomalous enhancement of charge density wave in kagome superconductor CsV_3Sb_5 approaching the 2D limit, Nature Comm. **14**, 2492 (2023).

[82] K. Koepernik and H. Eschrig, Full-potential nonorthogonal local-orbital minimum-basis band-structure scheme, Phys. Rev. B **59**, 1743 (1999).

[83] J. P. Perdew, K. Burke, and M. Ernzerhof, Generalized gradient approximation made simple, Phys. Rev. Lett. **77**, 3865 (1996).

[84] K. Momma and F. Izumi, *VESTA* 3 for three-dimensional visualization of crystal, volumetric and morphology data, J. Appl. Crystallogr. **44**, 1272 (2011).